Supplementary Information:

On the original layered OP4-$(Li,Na)_xCoO_2$ phase : insights on its structure, electronic structure and dynamics from solid state NMR

Yohan Biecher[a], Danielle L. Smiley[b], Marie Guignard[a], François Fauth[c], Romain Berthelot[d,e], Claude Delmas[a], Gillian R. Goward[b], Dany Carlier[a,e,]*

[a]CNRS, Univ. Bordeaux, Bordeaux INP, ICMCB UMR 5026, F-33600 Pessac, France

[b]Department of Chemistry & Chemical Biology, McMaster University, Hamilton, Ontario L8S 4M1, Canada

[c]CELLS - ALBA synchrotron, Cerdanyola del Vallès, E-08290 Barcelona, Spain

[d]CNRS, Univ. Montpellier, ICGM UMR 5253, F-34095 Montpellier, France ICGM, Université de Montpellier, CNRS, 34095 Montpellier, France

[e]Réseau sur le Stockage Electrochimique de l'Énergie (RS2E), CNRS, 80039 Amiens, France

** Corresponding author: dany.carlier@icmcb.cnrs.fr*

Figure S1: Comparison of the crystallographic data for the different OP4 phases reported in literature for various precursors. Note that the temperature used for the acquisition is not mentioned in the cited references.

Ref	Chemical formula	Space group	a_{hex} (Å)	c_{hex} (Å)	Precusors
1	$Li_{0.43}Na_{0.36}CoO_{1.96}$	$P6_3mc$	2.839(4)	20.36(3)	P2-$Na_{0.7}CoO_2$ + O3-$LiCoO_2$
2	$Li_{0.48}Na_{0.35}CoO_2$	$P6_3/mmc$	2.824	20.293	Na_2CO_3 + Li_2CO_3 + Co_3O_4
3	$Li_{0.41}Na_{0.31}CoO_2$	$P6_3mc$	2.8266(3)	20.265(2)	Na_2CO_3 + Li_2CO_3 + Co_3O_4
4	$Li_{0.42}Na_{0.36}CoO_2$	$P6_3mc$	2.839(4)	20.36(3)	Na_2CO_3 + Li_2CO_3 + Co_3O_4
5	$Li_{0.42}Na_{0.37}CoO_2$	$P6_3/mmc$	2.8301(2)	20.286(2)	P2-$Na_{0.7}CoO_2$ + O3-$LiCoO_2$
6	$Li_{0.48}Na_{0.35}CoO_2$	$P6_3mc$	2.821(3)	20.163(2)	P2-$Na_{0.7}CoO_2$ + O3-$LiCoO_2$
7	$Li_{0.42}Na_{0.36}CoO_2$	$P6_3mc$	2.831	20.26	P2-$Na_{0.7}CoO_2$ + O3-$LiCoO_2$
8	$Li_{0.37}Na_{0.31}CoO_2$	$P6_3/mmc$	2.8208(2)	20.277(1)	Na_2CO_3 + Li_2CO_3 + Co_3O_4

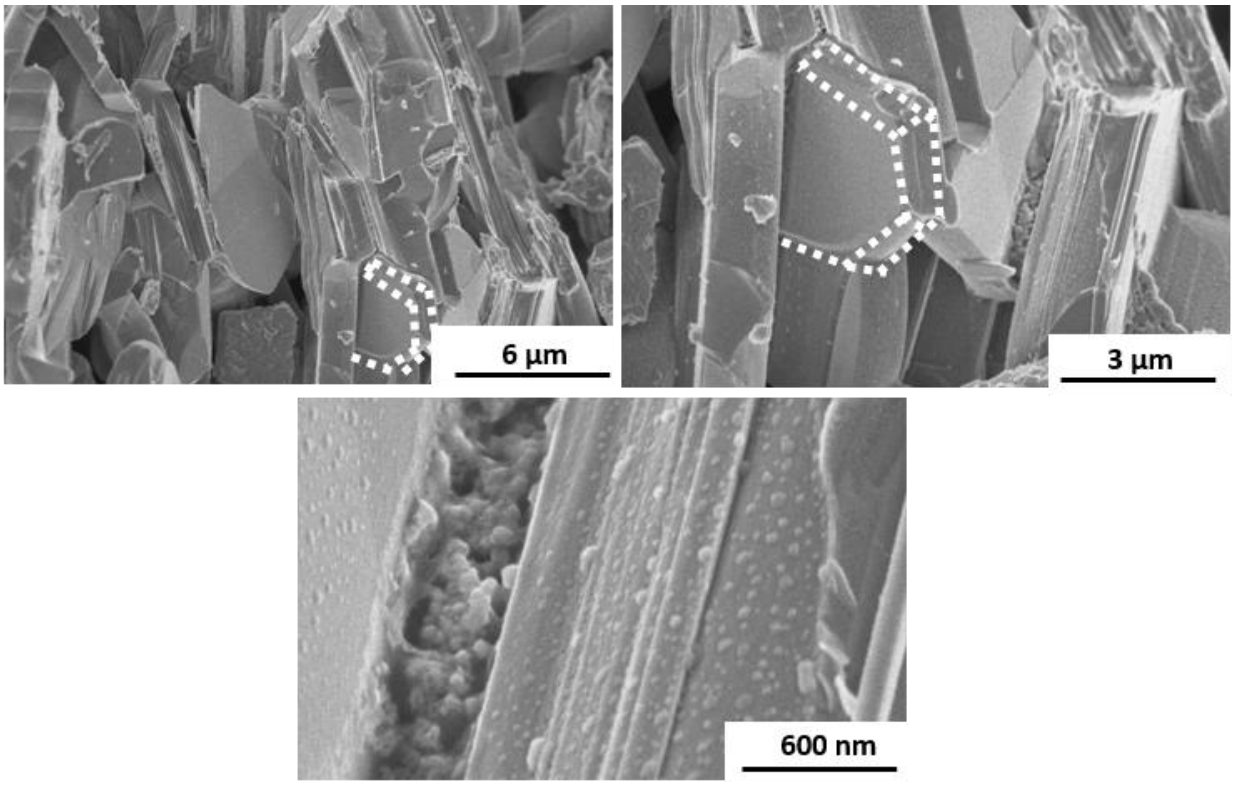

Figure S2 · SEM pictures of sample A at different

Figure S2: SEM pictures of the sample A at different magnifications. Dashed lines represent the shape of an OP4 crystal.

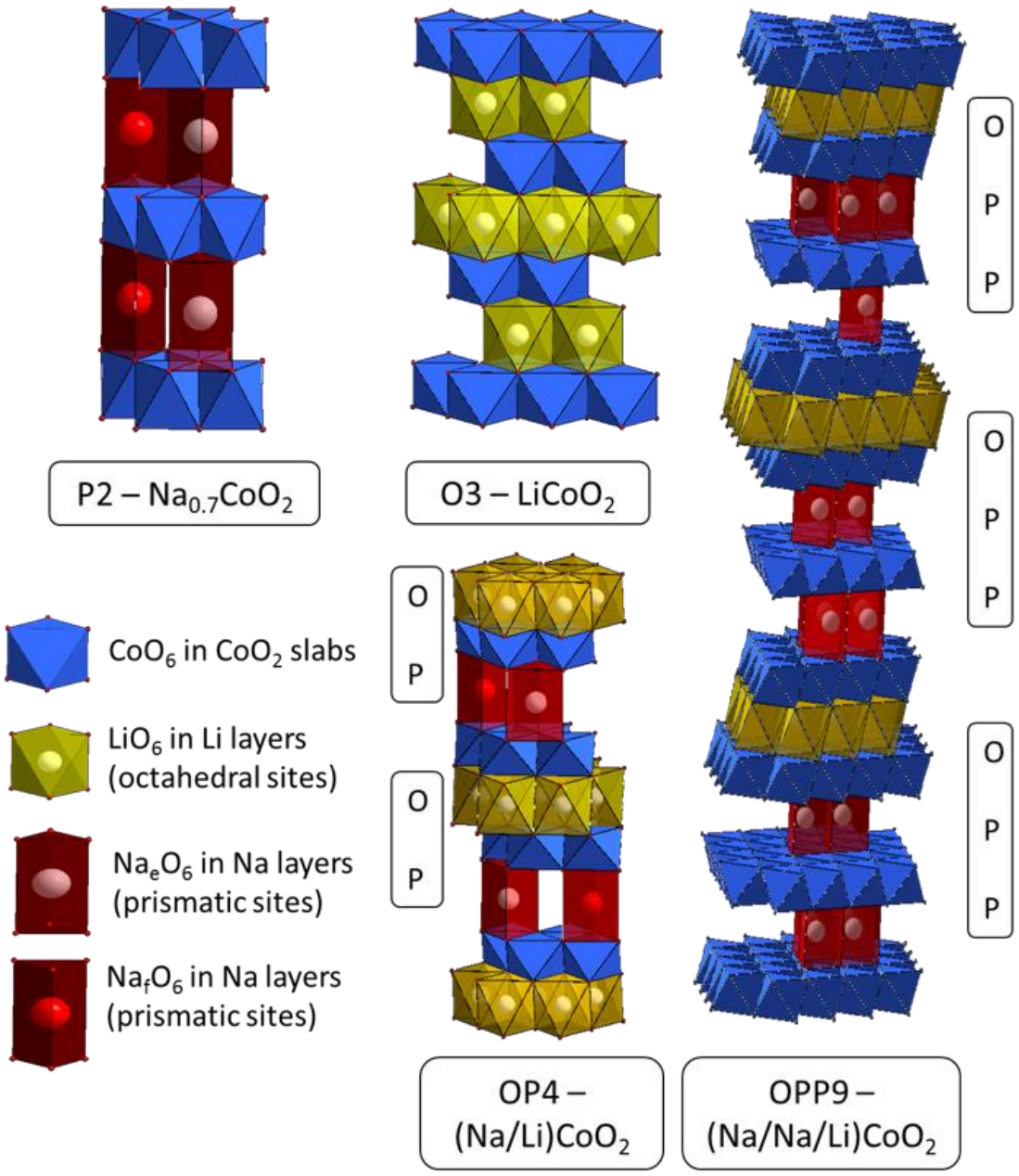

Figure S3: Representation of the different phases reported in this paper.

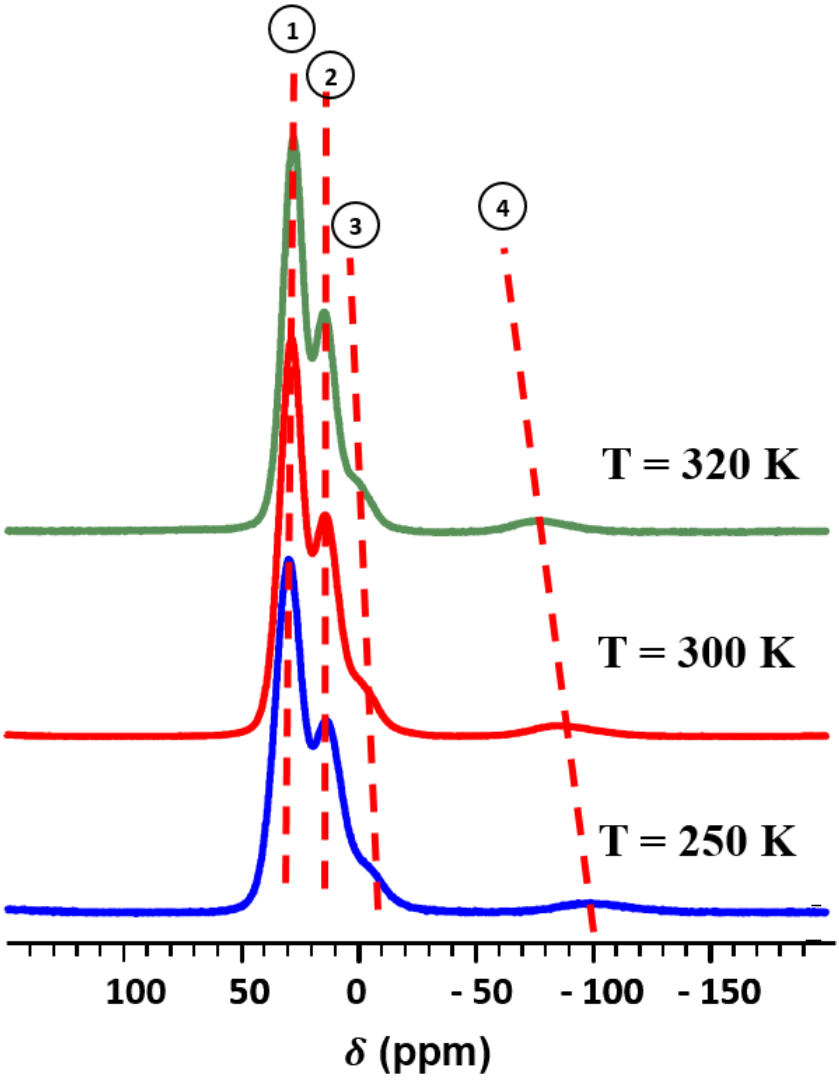

Figure S4: Experimental ^{7}Li MAS NMR spectra performed on a 7.05 T magnet with a spinning frequency of 30 kHz for 250 K, 300 K and 320 K.

S5: DFT calculations

A. Input

In order to propose a signals assignment of the positive and negative shifts observed, we have been using DFT calculations using PAW potentials allowing considering large supercells. First principles calculations were performed within the Density Functional Theory (DFT) framework. In a previous study, we showed that PAW-PBE potentials as implemented in the Vienna ab initio Simulation Package (VASP) code[9] can be used to compute theoretically the Fermi contact shifts in paramagnetic materials[10]. A plane wave energy cut-off of 600 eV and a k-mesh dense enough to reach convergence were used. All calculations were done with a ferromagnetic ordering which is considered appropriate for the Fermi contact shift, as described in reference 3. A model compounds was considered with the $Li_{0.5}Na_{1/3}CoO_2$ stoichiometry, considering a full Li layer as in O3-$LiCoO_2$ and the Na^+/vacancy ordering reported by Platova et al. for P2-$Na_{2/3}CoO_2$[11]. The description of this hypothetical cell can be found below in **Figure SI-5.1.** The supercell used corresponds to ($2\sqrt{3}*a_{hex.small}$, $2\sqrt{3}*a_{hex.small}$, $2c_{hex.small}$) with $a_{hex.small}$ and $c_{hex.small}$ the lattice vectors of the OP4 phase without considering a Na/vacancy ordering. For more clarity the vacancy position are note represented in Figure SI-5-1b, but the position of the Na_e and Na_f sites projection in the small hexagonal cell in provided in the inset. A quasi-Newton algorithm was used for ionic relaxations. To obtain accurate final energies, all relaxations were followed by a final static calculation with the linear tetrahedron method. In the Generalized Gradient Approximation (GGA), the inherent self-interaction error has detrimental effect on localized transition-metal d (or rare earth f) orbitals. Although, the addition of a Hubbard U correction can produce theoretical average voltages or Fermi contact shifts in better agreement with experiments[12], this method is not used in this study it has been shown to yield some unphysical results for layered cobalt oxide systems: phase stability

inversion between O1 and O3 in CoO_2 and incorrect phase diagram for the P2-Na_xCoO_2 system[13]. On the contrary, GGA has been successfully used to describe the phase diagram of the Li_xCoO_2 system[14]. The difficulty to properly model layered cobalt oxides probably comes from the dual character of the electronic properties: some electrons are fully delocalized leading to metallic conduction in plane[15] and some are localized leading to a Curie-Weiss type paramagnetism[16].

Equation (1) below is used to calculate this spin density, and uses the hyperfine coupling constant (A_{FC}) determined by VASP in addition to the total number of unpaired electrons in the unit cell and gyromagnetic ratio of the nucleus to which spin density is being transferred to determine the total amount of spin density at each Na nucleus.

$$\rho(0) = \frac{A_{FC}3S}{\mu_0 \hbar \gamma_I g_e \mu_B} \quad (1)$$

where μ_0 is the permeability of free space, $\hbar$ is the reduced Planck constant, γ_I is the gyromagnetic ratio of the NMR observed nucleus, g_e is the electron g-factor, and μ_B is the Bohr magneton. The expected paramagnetic contribution to the NMR shift can then be determined by taking into account the spin density at the nucleus ($\rho(0)$) and the magnetic susceptibility of the material (χ_M) according to Equation (2):

$$\delta_{iso,FC} = \frac{1}{3SN_A}\rho(0)\chi_M \quad (2)$$

B. Results

For the magnetic susceptibility we used $\chi = C/(T - \theta_{CW})$, with C and θ_{CW} determined from a linear fit of the inverse of the magnetic susceptibility ($1/\chi$) versus temperature using the modified Curie-Weiss law (**Figure 5b**).

Even if the stoichiometry is slightly different from the experimental one and even though in our GGA approach all cobalt ions are partially oxidized, calculations showed that considering a specific Na ordering tends to partially localize the charges and lead to slightly different Co ions. The global spin calculated in the cell is in agreement with the expected value for 1/6 LS-Co^{4+} (t_{2g}^5) and 5/6 LS-Co^{3+} (t_{2g}^6). We could further compute the expected Fermi contact shifts for the different Li and Na nuclei in the supercell using either the theoretical Curie constant (C_{th}=0.0625 emu.K.mol^{-1}) or the C_{exp} and θ Weiss experimental values obtained after fitting the magnetic susceptibility versus temperature curve. As expected from the larger C value experimentally observed, the resulting shifts magnitude is larger than using the theoretical C_{th}. Whatever the method used, the experimental data cannot be properly simulated **(Figure SI-5.2a**). This emphasizes the difficulty to model the electronic structure for layer cobalt oxides as discuss in the experimental part. In our modelling, the t_{2g} orbitals degeneracy is left because of the CoO_6 distortion along the c axis leading to a_{1g} and e_g' orbitals[17]. The 3D spin density maps show that the a_{1g} orbital is mainly carrying the spins (**Figure SI-5.3**). In reality the local electronic structure should be more complex and one expect some localized and some delocalized electrons in the t_{2g} orbital of the Co ions.

DFT calculations of the Fermi contact shifts for the different Na environments in the $Li_{0.5}Na_{1/3}CoO_2$ [$Na_{16}Li_{24}Co_{48}O_{96}$ supercell] model compound were also done. Only the computed positions of the isotropic peaks are shown on **Figure SI-5.2b** without any affected line shape. Fermi contact shifts computed for the Na_e sites are slightly lower than the ones computed for the Na_f sites. Since not

such broad distribution of isotropic shifts are observed experimentally, this further confirms the Na mobility is the sodium layers of the OP4 phase leading to an average signal and the assignment of the different signals to Na ions present in different layers or in different phases.

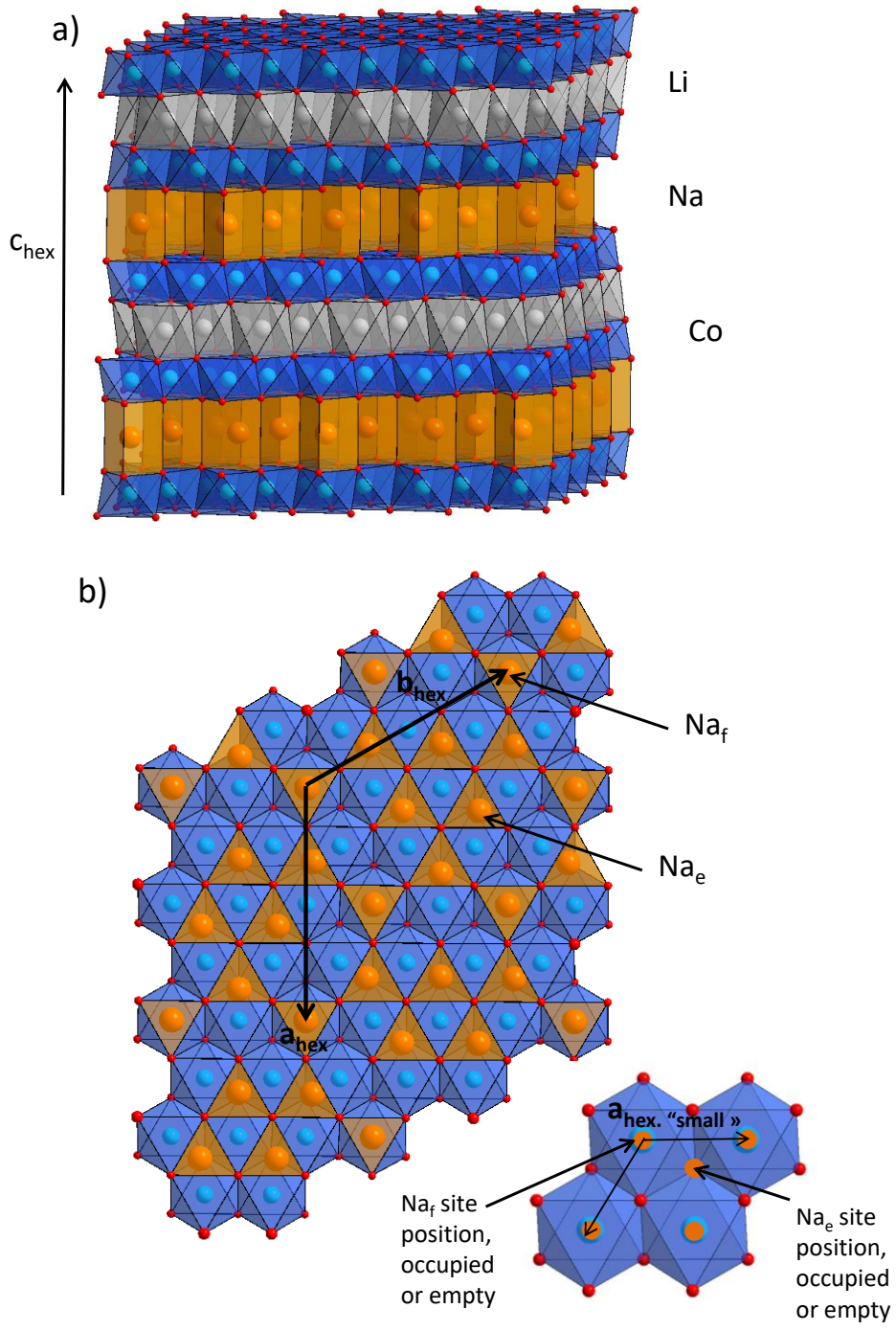

Figure S5.1: (a) Representation of the hypothetical cell $Li_{0.5}Na_{1/3}CoO_2$ used as model for DFT calculations. This model considers full Li layers and 67% filled Na layers. (b) Highlighting of the Na^+/vacancy ordering in the Na interslab spaces. In inset : projection of the position of the Nae and Naf sites in the "small" OP4 cell, i.e. before the construction of the supercell.

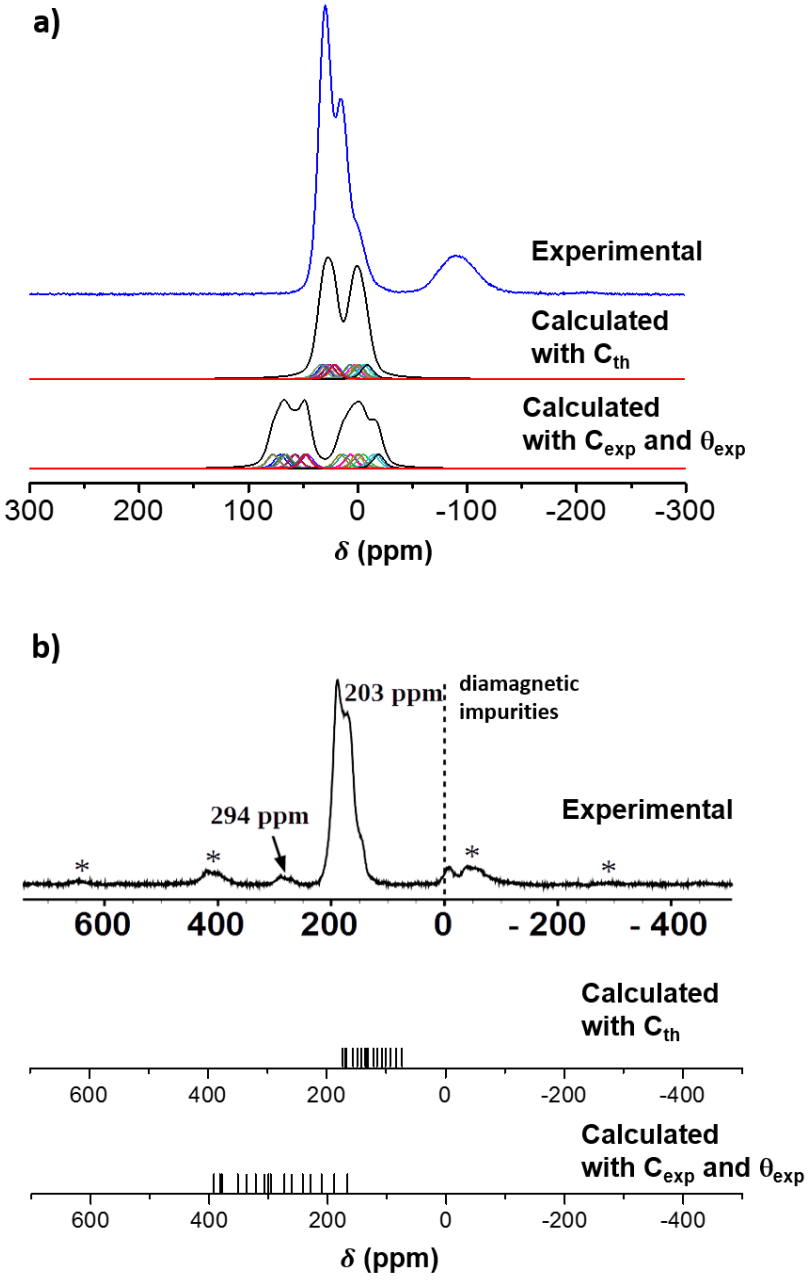

Figure S5.2: Comparison between experimental NMR spectra (Table 5) and calculated spectra considering theoretical curie constant and experimental one. (a) for ^{7}Li MAS NMR. (b) for ^{23}Na MAS NMR.

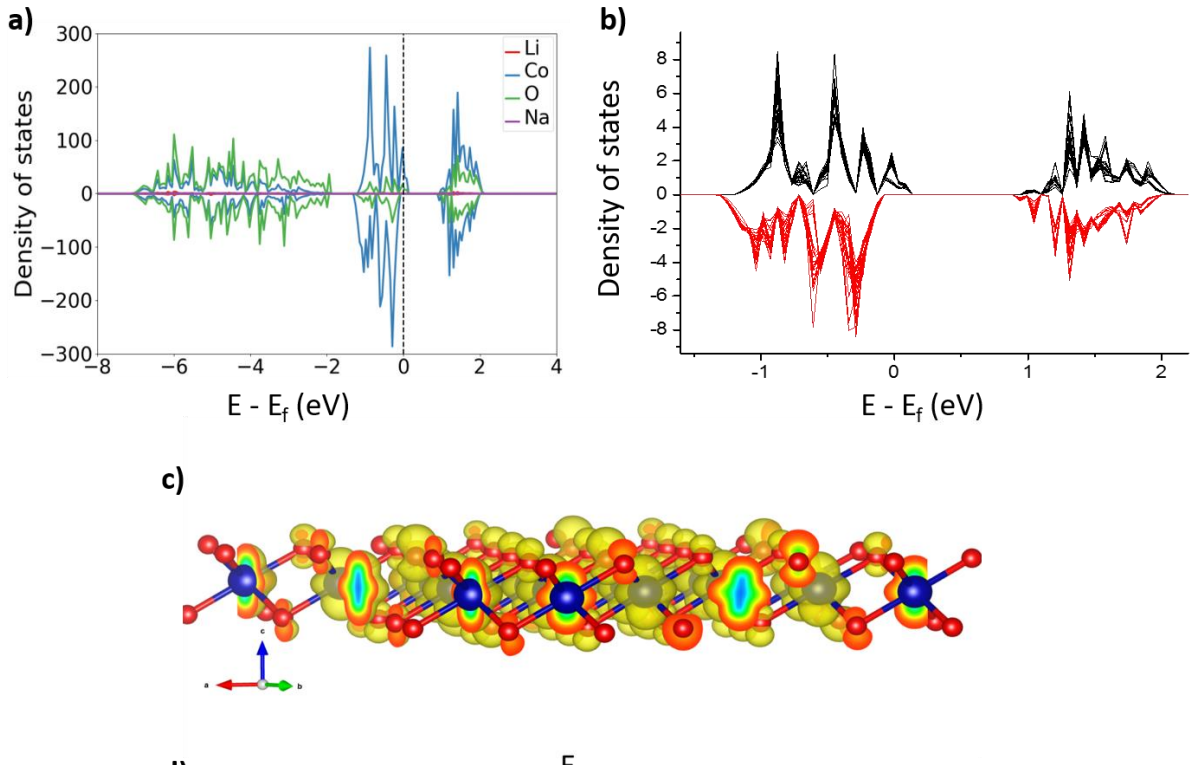

Figure S5.3: Calculated spin DOS of model presented in Figure SI-5.1. (a) total. (b) partial on Co 3d orbitals. (c) 3D spin density maps. a_{1g} orbital is mainly carrying the spins.

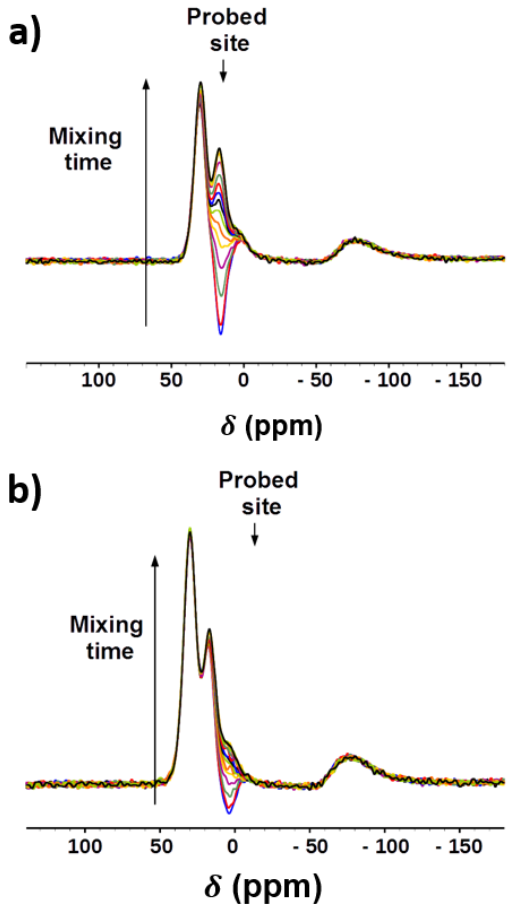

Figure S5 : Experimental ^{7}Li SI

Figure S6: Experimental ^{7}Li SI spectra performed at 340 K with mixing times from 0.05 ms to 6 s. (a) on site 2. (b) on site 3.

	δ_{iso} (ppm)	C_Q (MHz)	η	lb (ppm)
T = 270 K	217	4.08	0.16	15.8
T = 300 K	191	4.09	0.15	15.6
T = 350 K	166	4.12	0.02	14.2
T = 400 K	155	4.20	0.02	11.2
T = 450 K	148	4.25	0.06	10.6

Figure S7: Fitted parameters of the ^{23}Na MAS NMR spectra recorded while spinning at 13 kHz at variable temperatures (Figure 9). For each parameter the last number falls into the error bar. δ_{iso} (ppm) = the isotropic position ; C_Q (MHz) = the quadrupolar coupling; η = the assymetry parameter of the Quadrupolar interaction tensor and lb (ppm) = broadening factor.

References

(1) Balsys, R. J.; Davis, R. L. The Structure of $Li_{0.43}Na_{0.36}CoO_{1.96}$ Using Neutron Powder Diffraction. *Solid State Ion.* **1994**, *69* (1), 69–74.

(2) Ren, Z.; Shen, J.; Jiang, S.; Chen, X.; Feng, C.; Xu, Z.; Cao, G. Enhanced Thermopower in an Intergrowth Cobalt Oxide $Li_{0.48}Na_{0.35}CoO_2$. *J. Phys. Condens. Matter* **2006**, *18* (29), L379–L384.

(3) Bos, J. W. G.; Hertz, J. T.; Morosan, E.; Cava, R. J. Magnetic and Thermoelectric Properties of Layered $Li_xNa_yCoO_2$. *J. Solid State Chem.* **2007**, *180* (11),
(4) Semenova, A.; Kellerman, D.; Baklanova, I.; Perelyaeva, L.; Vovkotrub, E. Raman Spectroscopy Study of Sodium–lithium Cobaltite. *Chem. Phys. Lett.* **2010**, *491* (4–6), 169–171.
(5) Berthelot, R.; Pollet, M.; Carlier, D.; Delmas, C. Reinvestigation of the OP4-(Li/Na)CoO_2 -Layered System and First Evidence of the (Li/Na/Na)CoO_2 Phase with OPP9 Oxygen Stacking. *Inorg. Chem.* **2011**, *50* (6), 2420–2430.
(6) Kellerman, D. G.; Zhuravlev, N. A.; Semenova, A. S.; Shein, I. R.; Kuznetsov, M. V. ^{23}Na NMR in Binary Lithium-Sodium Cobaltite. *Bull. Russ. Acad. Sci. Phys.* **2011**, *75* (8), 1157–1159
(7) Mesilov, V. V.; Galakhov, V. R.; Semenova, A. S.; Kellerman, D. G.; Elokhina, L. V. X-Ray Spectra and Specific Features of the Structure of Lithium-Sodium Cobaltite $Li_xNa_yCoO_2$. *Phys. Solid State* **2011**, *53* (2), 271–275.
(8) Yabuuchi, N.; Kawamoto, Y.; Hara, R.; Ishigaki, T.; Hoshikawa, A.; Yonemura, M.; Kamiyama, T.; Komaba, S. A Comparative Study of $LiCoO_2$ Polymorphs: Structural and Electrochemical Characterization of O2-, O3-, and O4-Type Phases. *Inorg. Chem.* **2013**, *52* (15), 9131–9142.
(9) Kresse, G.; Furthmüller, J. Efficiency of Ab-Initio Total Energy Calculations for Metals and Semiconductors Using a Plane-Wave Basis Set. *Comput. Mater. Sci.* **1996**, *6* (1), 15–50.
(10) Bamine, T.; Boivin, E.; Boucher, F.; Messinger, R. J.; Salager, E.; Deschamps, M.; Masquelier, C.; Croguennec, L.; Ménétrier, M.; Carlier, D. Understanding Local Defects in Li-Ion Battery Electrodes through Combined DFT/NMR Studies: Application to $LiVPO_4F$. *J. Phys. Chem. C* **2017**, *121* (6), 3219–3227.
(11) Platova, T. A.; Mukhamedshin, I. R.; Alloul, H.; Dooglav, A. V.; Collin, G. Nuclear Quadrupole Resonance and X-Ray Investigation of the Structure of $Na_{2/3}CoO_2$. *Phys. Rev. B* **2009**, *80* (22).
(12) Aykol, M.; Kim, S.; Wolverton, C. Van Der Waals Interactions in Layered Lithium Cobalt Oxides. *J. Phys. Chem. C* **2015**, *119* (33), 19053–19058.
(13) Hinuma, Y.; Meng, Y. S.; Ceder, G. Temperature-Concentration Phase Diagram of P2 Na_xCoO_2 from First-Principles Calculations. *Phys. Rev. B* **2008**, *77* (22). h
(14) Van der Ven, A.; Aydinol, M. K.; Ceder, G.; Kresse, G.; Hafner, J. First-Principles Investigation of Phase Stability in Li_xCoO_2. *Phys. Rev. B* **1998**, *58* (6), 2975–2987..
(15) Ménétrier, M.; Saadoune, I.; Levasseur, S.; Delmas, C. The Insulator-Metal Transition upon Lithium Deintercalation from $LiCoO_2$: Electronic Properties and ^{7}Li NMR Study. *J. Mater. Chem.* **1999**, *9* (5), 1135–1140.
(16) Igarashi, D.; Miyazaki, Y.; Yubuta, K.; Kajitani, T. Precise Control of Na Content in the Layered Cobaltate γ-Na_xCoO_2. *J. Electron. Mater.* **2010**, *39* (9), 1669–1673.
(17) Landron, S.; Soret, J.; Lepetit, M.-B. An *Ab Initio* Evaluation of the Local Effective Interactions in the Na_xCoO_2 Family. *J. Phys. Condens. Matter* **2010**, *22* (34), 345603.